Transforming Porous Silica Nanoparticles into Porous Liquids with Different Canopy Structures for CO₂ Capture

Lisha Sheng, Zhenqian Chen,* Xin Wang, and Abdul Samad Farooq

Read Online

ACCESS | Metrics & More | Article Recommendations | Supporting Information

ABSTRACT: Porous liquids (PLs) have both liquid fluidity and solid porosity, thereby offering a variety of applications, such as gas sorption and separation, homogeneous catalysis, energy storage, and so forth. In this research, canopies with varying structures were utilized to modify porous silica nanoparticles to develop Type I PLs. According to experimental results, the molecular weight of canopies should be high enough to maintain the porous materials in the liquid state at room temperature. Characterization results revealed that PL_1_M2070 and PL_1_AC1815 displayed low viscosity and good fluidity. Both low temperature and high pressure positively influenced CO₂ capacity. The cavity occupancy resulted in poorer sorption capacity of PLs with branched canopies in comparison with that with linear canopies. Furthermore, the sorption capacity of PL_1_M2070 was 90.5% of the original CO₂ sorption capacity after 10 sorption/desorption cycles, indicating excellent recyclability.

1. INTRODUCTION

Carbon dioxide (CO₂) is produced massively due to the rapid development of modern civilization, for instance, by the combustion of coke, natural gas, and coal, in the fermentation of sugar and carbohydrate materials, in the manufacturing of lime and cement, and so on. Therefore, CO₂, one of the major greenhouse gases, has raised significant concerns about the relationship between anthropogenic CO₂ and global warming. It is estimated that over 30 billion tons of CO₂ are released every year into the atmosphere. Indeed, CO₂ emissions have been increasing year by year, causing ecological and environmental problems such as rising atmospheric temperatures and global warming.[1] Therefore, there is an urgent need to introduce efficient CO₂ capture and separation technologies for effectively reducing CO₂ emissions with the ultimate goal of achieving a carbon-neutral economy.[2−4]

Physisorption, chemisorption, and membrane separation are prevalent CO₂ capturing technologies.[5,6] The physisorption method using porous materials as solid adsorbents is deemed an environmentally friendly and economically viable technique because of its minimum energy consumption and renewable advantages. So far, researchers have utilized several porous solid adsorbents for CO₂ sorption, including zeolites,[7] metal−organic frameworks (MOFs),[8] porous polymers,[9−12] porous carbon,[13−16] and porous silica.[17,18] Porous solids are well equipped with high porosity and diverse functionalities, resulting in superior carbon capture and selective sorption properties and low regeneration energy consumption. All of the characteristics point to a promising application for carbon capture. However, the solid nature of these materials poses

certain degrees of restrictions on their processing, transport, and integration into engineering systems for large-scale utilization.

The chemisorption method employs alcohol amine as an absorbent, such as ethanolamine[19] and methyldiethanol-amine.[20] The absorbents could be transported continuously with a pump, and the liquid circulation could be easily integrated into the existing factory process.[21] Alkanolamine solution is widely used in industrial decarbonization because of its large sorption capacity and high efficiency. However, it could react with CO₂ because of its low alkalinity, and volatilization and degradation of the resultant should cause equipment corrosion. Meanwhile, high regeneration energy consumption might hinder the long-term application.[22,23]

Porous liquids (PLs) were first proposed by James and co-workers in 2007,[24] which combined porosity with fluidity. As the novel class of materials, they deemed broad application prospects in gas sorption and separation.[25−27] PLs can be categorized into three types based on their characteristic.[28−30] Type I PLs were neat liquids that could not collapse or interpenetrate,[31−33] Type II PLs were porous molecule cages dissolving in steric solvents that were too bulky to enter the
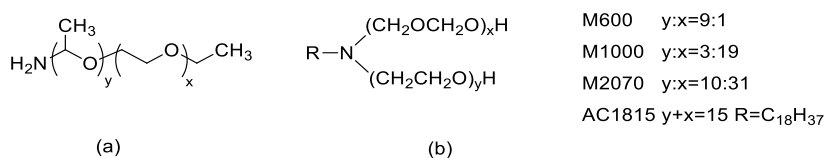
Figure 1. Chemical structures of canopies: (a) M600, M1000, and M2070; (b) AC1815.

cavities,[34−39] and Type III PLs were microporous framework particles dispersed in steric solvents.[40−43]

Type II PLs and Type III PLs were composed of a steric solvent and porous rigid body, which should be too bulky to enter the cavity. Giri et al.[44] modified porous organic cages (POCs) with alkanes to achieve fluidity, but polymer chains would occupy the nonporous cavities of POCs. Afterward, Giri et al.[45] modified POCs with a crown ether group and then dissolved modified POCs into 15-crown-5 solvents to form Type II PLs. Experimental results showed that the viscosity of PLs was ranged from 20 →140 cP at 298−323 K, depending upon the concentration of POCs. PLs had higher viscosity, a more complex reaction process, and a lower yield when compared to the corresponding solvent 15-crown-5 (8.9−22.4 cP) (3.1−6.5%). Based on the aforementioned shortcomings, Mastalerz et al.[46] proposed a simple, cost-effective procedure that involved replacing the original 1,2-ethylenediamine with a binary amine mixture and employing another hexachloropropene with higher mobility and solubility as the potential steric solvent. Deng et al.[33] successfully dissolved the metal−organic polyhedron (MOP-18) in 15-crown-5 to prepare Type II PLs at room temperature. The temperature affected the solubility of the core. At 60 °C, PLs with 30% core content could be obtained, while the core precipitated at a specific time at 25 °C. A stable PL with a low core content could be obtained at 40 °C. Both molecular dynamics simulation and experimental characterization revealed that the cavities of MOP-18 were not occupied by the 15-crown-5 solvent, which has high CO_2 solubility and could be used for CO_2 sorption.

Shan et al.[31] developed Type III PLs by employing ZIF-8, ZSM-5, and silicalite-1 as the core, with bulky ionic liquids ([DBU-PEG][NTf2]) acting as steric solvents. The size effect completely blocked the larger cation of the ionic liquid outside the cavities owing to quantum chemistry results. The corresponding anion could not enter the cavity despite their small size due to the intense electrostatic interaction energy between the cation and anion of ionic liquids, leaving cavities unoccupied in solvents. Li et al.[47] employed a similar strategy to fabricate PLs by dispersing polymer amine (D2000) and modified MOFs (UiO-66) in ionic liquids. Experimental results showed that the CO_2 uptake value of PLs increased from 2.86 to 7.32 wt % when the mass ratio of porous UiO-66 increased from 0 to 50 wt %, which implied that the CO_2 uptake value of PLs was approximately three times that of the corresponding ILs. Li[48] employed UiO-66 as the pore carrier and poly(dimethylsiloxane) as the bulky solvent to form Type III PLs. Sorption experiments showed that CO_2 uptake capacity decreased with the decrease in the MOF content.

Dai and co-workers[31] successfully prepared Type I PLs for the first time by modifying hollow silica nanoparticles with poly(ethylene glycol)-tailed sulfonate. Another study[32] utilized the electrostatic interaction between carbon networks and polymerized ionic liquids to create carbon-based PLs. The CO_2 uptake value of the PLs at 1 bar was 0.445 wt %, which was much higher than that of corresponding polymerized ionic

liquids (0.261 wt %). Furthermore, they developed similar PLs by transforming POCs into PLs via a supramolecular complexation strategy, but the sorption capacities of PLs (∼ 0.4 mmol/g) were significantly lower than those of the corresponding porous solids (1.062 mmol/g).[49]

Although several different kinds of PLs have been synthesized for gas capacity and separation, corresponding CO_2 sorption experiments were rarely performed. Herein, we first synthesized Type I PLs with the core of large porous silica nanoparticles (PSNs) rather than hollow silica nanoparticles, which had previously been theoretically demonstrated by molecular dynamics (MD) simulations.[25−27] Scanning electron microscopy (SEM), transmission electron microscopy (TEM), pore size analysis, Fourier transfer infrared (FT-IR) spectroscopy, and thermogravimetric analysis were performed for characterization, and the effects of temperature, pressure, and canopy structures on absorptivity were investigated.

2. EXPERIMENTAL SECTION

2.1. Materials. Methanol (AR, 99.5%, MeOH), cetyltrimethylammonium bromide (CTAB), deionized water, and ethanol (AR, EtOH) were purchased from Sinopharm Chemical Reagent Co., Ltd., γ-(2,3-epoxypropoxy)-propytrimethoxysilane (KH560), tetraethyl orthosilicate (TEOS), and ammonia ($NH_3·H_2O$) were purchased from Aladdin Chemistry Co., Ltd., ethoxylated amine (AC1815, Mw ∼ 1000) and polyether amine (Jeffamine M600, Mw ∼ 600, Jeffamine M1000, Mw ∼ 1000, Jeffamine M2070, Mw ∼ 2000) were purchased from Shanghai Longquan Chemical Technology CO., Ltd.

2.2. Synthesis of PLs. The synthesis of PLs could be divided into two steps: the formation of PSNs and the formation of PLs. PSNs were created based on previously reported work with a few changes.[50] First, a solution of 64 mL of H_2O, 25 mL of EtOH, and 2.6 g of CTAB was stirred for 30 min at 60 °C. After adding 0.55 mL of aqueous $NH_3·H_2O$, 8 mL of TEOS was added to the above solution within 5 min and stirred for 2 h. The sample was purified by washing it several times with deionized water and EtOH before drying it at 60 °C for 10 h. Finally, white PSNs could be obtained by calcinating precursors in an air atmosphere at a heating rate of 1 °C/min for 5 h at 550 °C.

PSNs were then functionalized by coronas (KH560) and canopies (branched ethoxylated amine: AC1815; linear polyether amine: Jeffamine M600, Jeffamine M1000, and Jeffamine M2070) to produce PLs, and the chemical structures of canopies are shown in Figure 1. In general, a unit of Type I PLs consisted of a surface-functionalized nanoparticle as a core to which selected polymers were tethered to form a canopy. Such a configuration could provide the fluidity of PLs, prevent loss of polymers, and enable PLs to exhibit near zero vapor pressure. Initially, KH560 was added dropwise to the canopy (15% in MeOH) solution, which was then stirred for 12 h at a temperature of 50 °C. The PSN suspension was then prepared with the MeOH solution and sonicated for 30 min. Next, the

suspension was added to the above solvent and stirred for 24 h at 50 °C. The mixed solution was then dialyzed against deionized water for 72 h, with water exchanged every 24 h, using a preswollen dialysis membrane (Spectra/Por CE dialysis tubing, 3500-5000MWCO). Finally, PLs were obtained by centrifugation and drying at 50 °C for at least 120 h. PLs modified with M600, M1000, M2070, and AC1815 were labeled as PL_1_M600, PL_1_M1000, PL_1_M2070, and PL_1_AC1815, respectively. Details of the amounts of PSN, KH560, and canopies are listed in Table 1.

Table 1. Reaction Conditions To Synthesize PLs

samples	KH560 mass (g)	canopy type	canopy mass (g)	PSN mass (mg)
PL_1_M600	0.9456	M600	2.4	0.4
PL_1_M1000	0.9456	M1000	4	0.4
PL_1_M2070	0.9456	M2070	8	0.4
PL_1_AC1815	0.9456	AC1815	4	0.4

2.3. Characterization Methods. FT-IR spectra were measured with a Thermo Scientific Nicolet iS5 spectrometer. Thermogravimetric analysis (TGA) was performed with a TGA 5500 instrument under an N_2 atmosphere with a heating rate of 5 °C/min and a temperature range of 20−550 °C. SEM images were obtained using a JSM7800F instrument, and TEM observations were obtained using a JEOL JEM 2100PLUS instrument. Nitrogen sorption isotherms at 77 K were used to obtain pore structure information, including specific surface area, pore size distribution, and pore volume. The viscosity was measured using a HAKKE MARS60 at temperatures ranging from 10 to 60 °C and a heating rate of 2 °C/min.

2.4. CO_2 Sorption/Desorption Experiments. A CO_2 sorption system was employed to investigate the CO_2 sorption/desorption performance of PLs, and it primarily consisted of a 50 mL buffer chamber, a 25 mL sorption chamber with a magnetic stirrer, a temperature control system, two pressure sensors, and a vacuum pump, as shown in Figure 2. The detailed experimental process and calculation method are introduced in the Supporting Information.

2.5. Numerical Fitting. There are several sorption kinetics models being developed to investigate the sorption process and mass transfer mechanisms.[51,52] In this paper, the pseudo-first-order model and pseudo-second-order model were employed to investigate the mechanisms for CO_2 sorption in PLs, which were suitable to predict the combination of physisorption and chemisorption, respectively.[53,54] The kinetic equations were given as follows.

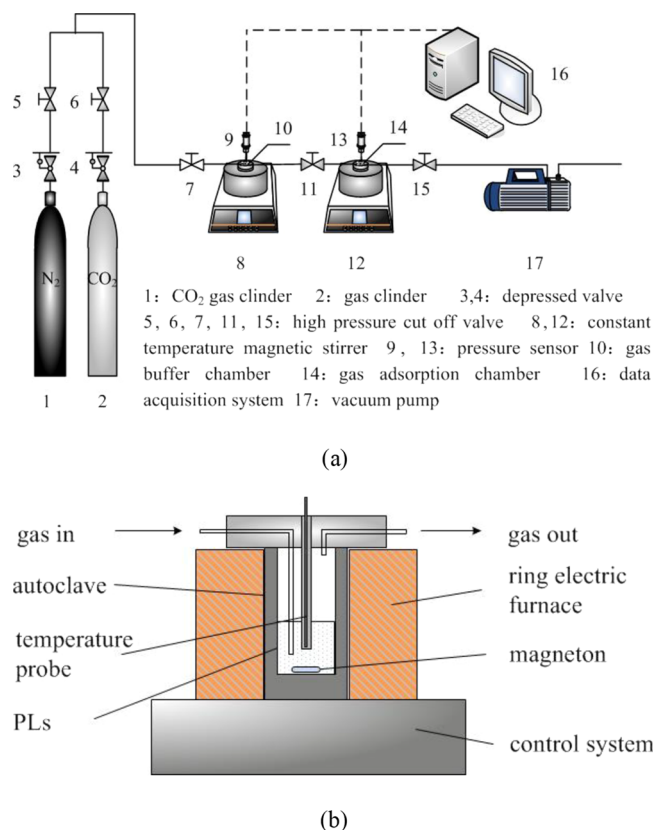The pseudo-first-order kinetic equation:

$$q_t = q_e(1 - e^{-k_1 t}) \tag{1}$$

The pseudo-second-order kinetic equation:

$$q_t = \frac{k_2 q_e^2 t}{1 + k_2 q_e t} \tag{2}$$

where k_1 and k_2 are rate constants in min^{-1}, and q_t and q_e are the sorption capacity at a given time t (min) and equilibrium time in mmol-CO_2/g-sorbent, respectively.

3. SIMULATION SECTIONS

3.1. Molecular Modeling. A PL model was built to further understand the stability and gas diffusion capacity, as shown in

1: CO_2 gas clinder   2: gas clinder   3,4: depressed valve   5, 6, 7, 11, 15: high pressure cut off valve   8,12: constant temperature magnetic stirrer   9, 13: pressure sensor   10: gas buffer chamber   14: gas adsorption chamber   16: data acquisition system   17: vacuum pump

(a)

(b)

Figure 2. (a) Schematic view of the gas sorption system; (b) structure of the sorption chamber.

Figure 3. The detailed PL model with a grafting density of 0.25 and pore radius of 12 Å was introduced in our previous work.[25]
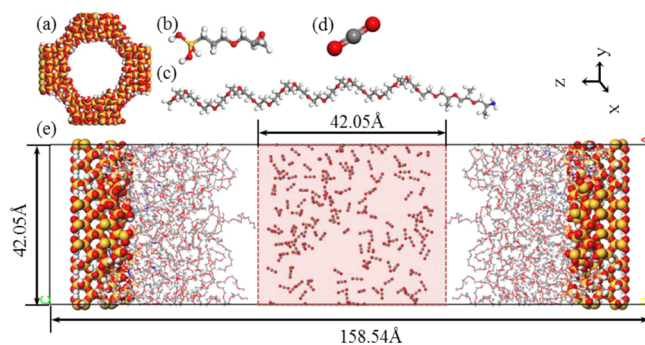
Figure 3. Molecular models of CO_2 capture in porous liquids. Molecular models of (a) hollow silica nanoparticle surfaces; (b) corona, KH560; (c) canopy, M1000; (d) CO_2 gas molecule; (e) CO_2 capture model.

The rigid and linear CO_2 was modeled with a bond length C−O of 1.16 Å and with partial charges of $q_O = -0.4e$ and $q_C = 0.8e$. The COMPASS force field was used in the simulation to describe the interactions of PLs and CO_2.

3.2. Simulation Methods. MD simulations were performed by Material Studio 2018. First, the PL surface was annealed in NVT ensemble using a Nose thermostat. Annealing cycles were set 10 with an initial temperature of 310 K and mid-cycle temperature of 500 K. Heating ramps of each cycle were 20, and dynamics steps per ramp were 200. The model was geometry optimized after each cycle to achieve

a reasonable surface. Then, a CO_2 cube box with a length of 42.05 Å at a temperature of 310 K and pressure of 60 bar was built by the Amorphous Cell module. Finally, MD simulations were carried out at 310 K with a time step of 1 fs in NVT ensemble using a Nose thermostat under 3D periodic boundary conditions. The initial velocity obeyed Maxwell distribution. The atom-based summation method and Ewald summation method were used respectively to compute van der Waals force and electrostatic force with a cutoff radius of 15.5 Å. Based on the convergence of potential energy and temperature, MD simulation time was 8 ns with a time step of 1 fs, information was collected in every 5000 steps, and the final 5 ns was used for producing the statistical computations. Potential energy and temperature vs dynamics time is shown in Supporting Information Figure S1. For example, the potential energy and temperature of CO_2 capture in PL vs dynamics time fluctuated in the range of 5~10% at the end of simulation, which indicated that the MD simulation was long enough to get reliable conclusions.

3.3. Translation Diffusion Coefficients. The mass transport coefficient was calculated by the Einstein relationship:[25]

$$D = \lim_{t \to \infty} \frac{1}{6t} \langle |\vec{r}(t) - \vec{r}(0)|^2 \rangle \tag{3}$$

where $r(t)$ is the position vector of the atoms from 0 to t. The diffusion coefficient could be fit by the slope of the mean square displacement (MSD).

4. RESULTS AND DISCUSSION

4.1. Characterization of PLs. Figure 4 represents the actual state of PLs with varying canopy structures. It was
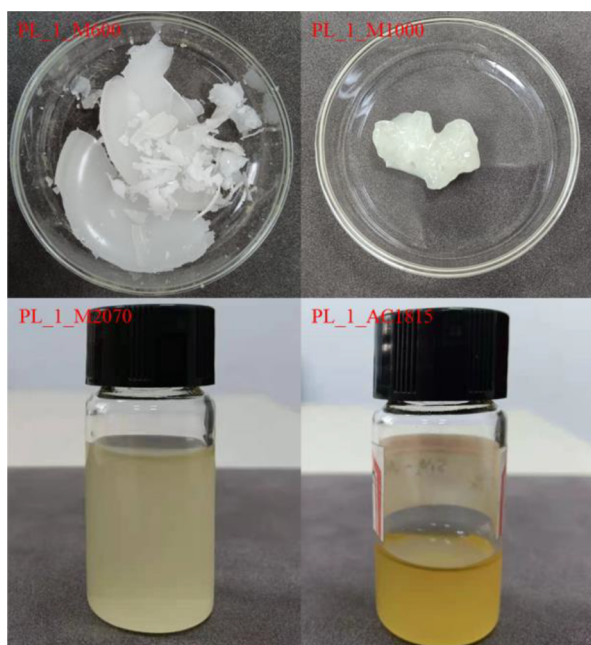

Figure 4. Actual state of PLs with different canopy structures.

demonstrated that the porous materials with various canopy structures were not always in the liquid state. PL_1_M600 was a white amorphous solid at room temperature with debris after touching, while PL_1_M1000 had a gel-like appearance and high viscosity. At room temperature, PL_1_M2070 exhibited a

light yellow liquid state, whereas the color of PL_1_AC1815 was slightly darker than that of PL_1_M2070, which was primarily due to the color difference of the grafted canopy.

N_2 sorption isotherm and pore size distribution of PSNs are shown in Supporting Information Figure S2. SEM and TEM were used to characterize the morphology of PSNs and PLs. Pure PSNs exhibited a relatively concentrated particle size distribution and aggregated together (Supporting Information Figure S3). However, canopies surrounded the cores of PLs, and nanoparticles were well dispersed with no apparent aggregation, as shown in Figure 5. It was primarily because the
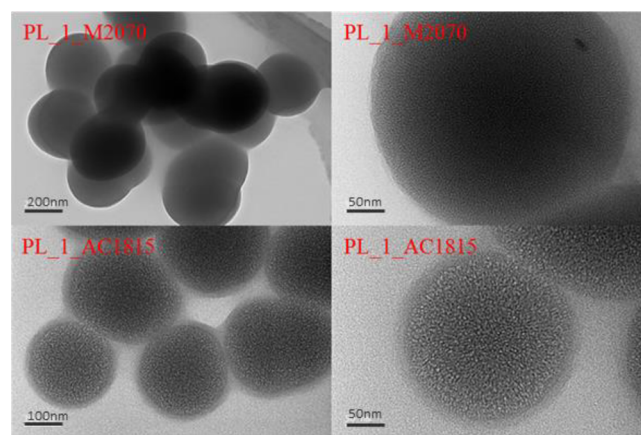

**Figure 5.** TEM images of PLs with different canopy structures.

canopies took up a certain free space between the cores. Once the cores were close to each other, the free space between them was squeezed and the steric hindrance of the polymers separated the nanoparticles from each other, preserving the dispersion stability of the PLs, as previously demonstrated by our simulation results.[25]

Figure 6 depicts the FT-IR spectrum of PLs with various canopies. Except for the existing peaks of pure cores, it was demonstrated that PLs had other peaks. For example, the antisymmetric stretching vibration peak of Si−O−Si near 1090 cm^{-1} and the antisymmetric stretching vibration peak of −OH at 3496 cm^{-1} in the FT-IR spectrum were the core characteristic peaks in PLs. Meanwhile, there was an H−O−H bending vibration peak at 1640 cm^{-1}, which validated the existence of water in PLs. In addition, there were a C−H stretching vibration peak at 2864 and 2920 cm^{-1} and an N−H stretching vibration peak at 3200−3500 cm^{-1}, which were canopies' characteristic peaks. The antisymmetric stretching vibration peak of −OH at 3496 cm^{-1} was weakened compared to pure cores, owing to the partial consumption of −OH during the bonding process between coronas and cores. Similarly, compared to pure M2070,[55] the N−H stretching vibration peak of PLs at 3200−3500 cm^{-1} was significantly weakened because of the combination of primary amino groups of canopies and epoxy propyl groups of coronas consuming part of the N−H bond during the preparation process, confirming the successful work of PLs from the side.

The TG analysis of PLs and pure M2070 is shown in Figure 7. M2070 began to decompose at 217.5 °C and completely decomposed when the temperature reached 300 °C.[55] The initial decomposition temperature of PLs with different canopies, on the other hand, was all-around 300 °C, and the decomposition process ended at around 400 °C. Therefore, the
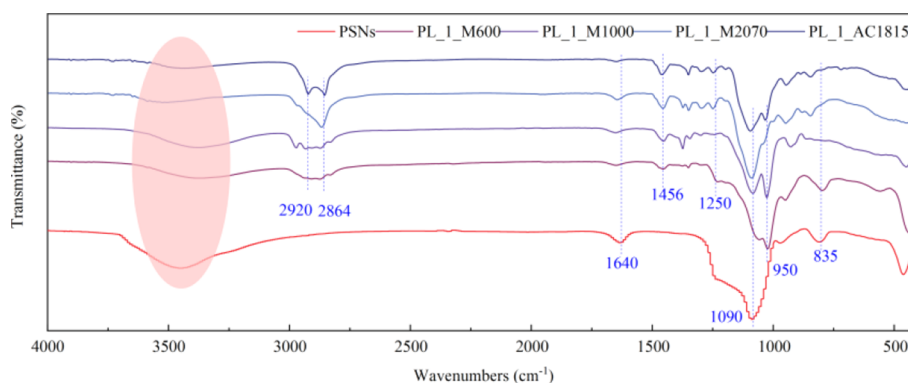
**Figure 6.** FT-IR spectrum of PLs and corresponding PSNs.
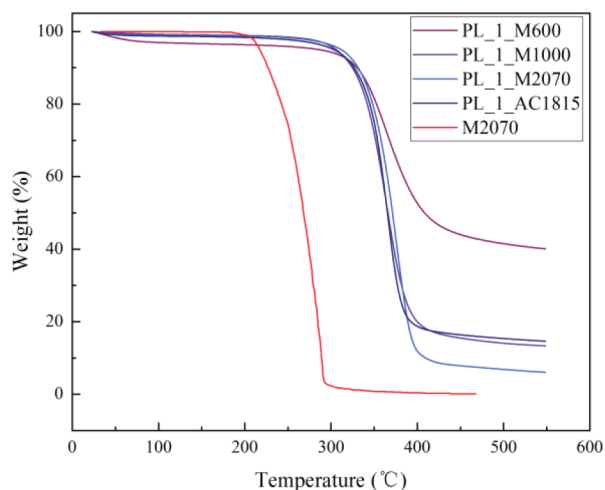
Figure 7. TGA curve of PLs and pure M2070.

PL was more stable than pure polyether amine. Meanwhile, at the end of the decomposition process, the solid content of PL_1_M600, PL_1_M1000, PL_1_M2070, and PL_1_AC1815 was 40.01, 13.31, 6.1, and 14.61%, respectively. The higher the polymerization degree of the canopies, the lower the solid content of the corresponding PLs, resulting in different solid–liquid ratios of the PLs when prepared with the same molar ratio of the core to the canopy. The highest solid

content was PL_1_M600, an amorphous solid, followed by PL_1_M1000, a glassy state gel. PL_1_M2070 had the lowest solid content and was liquid at room temperature. Furthermore, PL_1_M1000 and PL_1_AC1815 had similar solid contents but different states, indicating that the branched structures also affected the PLs' state.

The viscosity curves of canopies and PLs vs temperature are shown in Figure 8. The viscosity of the canopy and PLs decreased with increasing temperature, exhibiting typical fluid properties.[56] When the temperature was raised, the state of M600 changed from solid to liquid with the viscosity changing dramatically. M2070 > M1000 > AC1815 > M600 was the order of viscosity of canopies from high to low when the temperature was higher than 20 °C.

From Figure 8b, the viscosity of PLs was much higher than that of the corresponding canopies, but the difference decreased as temperature increased. At 25 °C, the viscosity of M2070 and AC1815 was 295.9 and 229.8 mPa·s, respectively. However, the viscosity of PL_1_M2070 and PL_1_AC1815 was 916.6 and 601.1 mPa·s, respectively. It was found that the viscosity of canopies and PLs was affected by both branches and degrees of polymerization. The molecular weight increased as the degree of polymerization increased, entanglement occurred, the mutual displacement between molecules became difficult, flow resistance increased, and viscosity increased. The branches of PLs had a significant influence on viscosity when their molecular weight was similar.
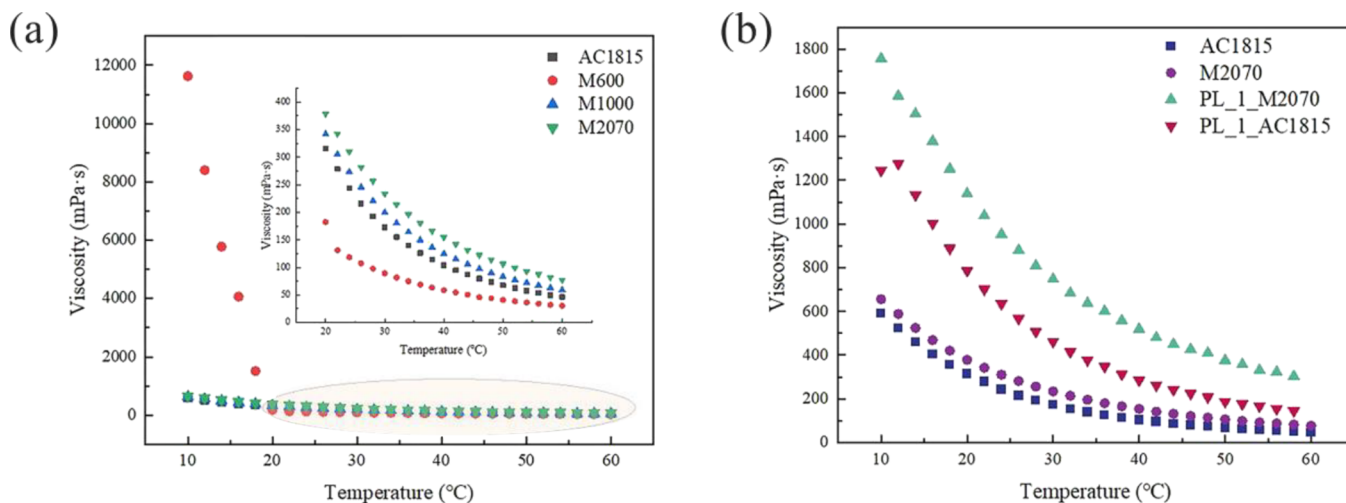
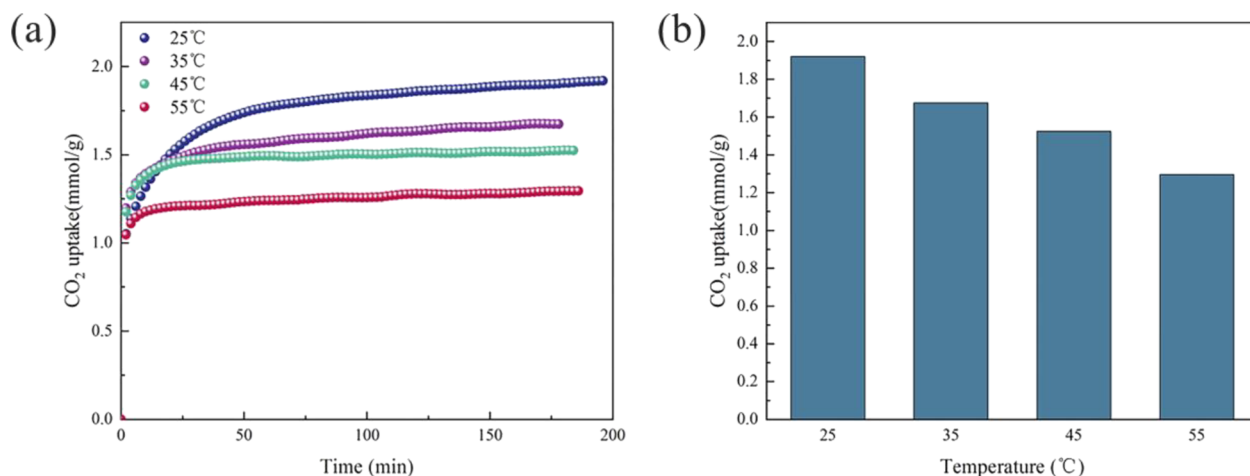**Figure 8.** Viscosity of pure canopies and PLs. (a) Pure canopy; (b) PLs.

Figure 9. CO_2 sorption performance of PL_1_M2070 at different temperatures: (a) sorption kinetics curve; (b) sorption amount.
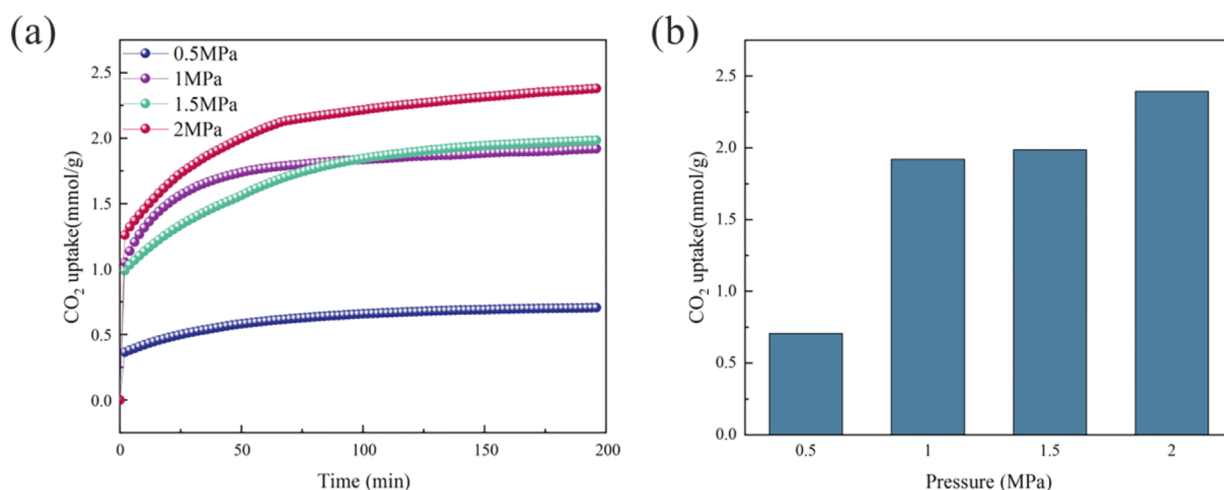

Figure 10. CO_2 sorption performance of PL_1_M2070 at different pressures: (a) sorption kinetics curve; (b) sorption amount.

Because of the presence of branches, the possibility of entanglement between canopies was reduced, as was flow resistance.[57] As a result, the viscosity decreased, and the fluidity of PLs improved.

4.2. CO_2 Sorption/Desorption Performance. The temperature was a significant factor in gas sorption kinetics. Figure 9 depicts the CO_2 sorption kinetics curve and sorption amount of PL_1_M2070 at various temperatures. At 25, 35, 45, and 55 °C, the sorption capacity of PL_1_M2070 was 1.920, 1.674, 1.525, and 1.295 mmol/g, respectively, which decreased with increasing temperature. It was primarily because increasing the temperature inhibited the dissolution and reaction of PLs with CO_2, lowering the saturation sorption capacity of CO_2.

The sorption mechanisms of PLs at different temperatures were studied using a pseudo-first-order model and a pseudo-second-order model. Supporting Information Table S1 shows the parameters fitted by the kinetic model. Under different temperature conditions, the correlation coefficient R^2 of the pseudo-second-order kinetic model fitting experimental data (0.9730−0.9886) was higher than the correlation coefficient R^2 of the pseudo-second-order fitting experimental data (0.9108−0.9757), indicating that the pseudo-second-order kinetic model was better suited to describe the sorption behavior.

This shows that there was not only physisorption but also chemisorption in the CO_2 sorption of PL_1_M2070.

The pressure was another important factor influencing the gas sorption process. Figure 10 depicts the CO_2 sorption kinetics curves and sorption amount of PL_1_M2070 at various pressures. At 0.5, 1, 1.5, and 2 MPa, the sorption amount of PL_1_M2070 was 0.706, 1.920, 1.987, and 2.393 mmol/g, respectively. The CO_2 sorption process by PL_1_M2070 was a combination of physical dissolution and chemisorption because the amount of physical dissolution increased with increasing pressure, and the total sorption capacity of CO_2 increased.

The sorption mechanism of PLs at different pressures was studied using a pseudo-first-order model and a pseudo-second-order model. Supporting Information Table S2 shows the parameters fitted by the kinetic model. The equilibrium sorption capacity fitted by the pseudo-second-order kinetic model was found to be greater than that fitted by the pseudo-first-order kinetic model under different temperature conditions. Meanwhile, the correlation coefficient R^2 of the pseudo-second-order kinetic model fitting experimental data was 0.9471−0.9742, greater than the correlation coefficient R^2 of the pseudo-first-order kinetic model fitting experimental data (0.8918−0.9108), indicating that the pseudo-second-order kinetic model was better suited to describe sorption
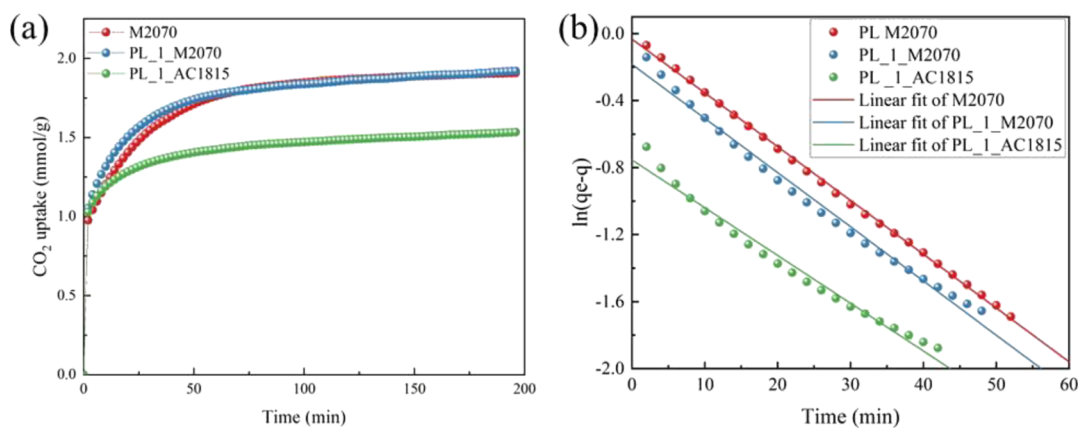
Figure 11. PLs with different canopy structures: (a) CO_2 sorption kinetics curves; (b) sorption fitting curves.

behavior. It was again confirmed that the quasi second-order kinetic model could better reflect the CO_2 sorption of PL_1_M2070. Results showed that there was not only physisorption but also chemisorption in the CO_2 sorption process.

Since PL M600 and PL M1000 were not fluid at room temperature, the following analysis focused on PL_1_M2070 and PL_1_AC1815. Figure 11 depicts CO_2 sorption curves of PLs with various canopy structures, and Supporting Information Table S3 lists the equilibrium sorption capacity and sorption rate obtained from the pseudo-second-order model sorption kinetic model. The sorption amount of CO_2 of pure M2070, PL_1_M2070, and PL AC1815 was 1.9085, 1.9207, and 1.5377 mmol/g, respectively, as shown in Figure 10. Results showed that the CO_2 sorption capacity of PLs was not superior to that of their corresponding canopy, which appeared to contradict the following results.[58] It was concluded from ref 58 that the branched structure caused the canopies to be orderly arranged. As a result, nanoparticle organic hybrid materials with less volume swelling could achieve higher CO_2 loading. However, because the pore size of the PLs prepared in this paper was larger, canopies could quickly enter the cavities of the cores, reducing the CO_2 sorption site and capacity. Furthermore, the amount of CO_2 absorbed by PL_1_M2070 was more significant than that by PL_1_AC1815 because branched canopies were easier to enter the cavities of PLs than linear canopies, as evidenced by our MD simulation results.[18]

In addition, damping film theory was used here to estimate the sorption rate.[59] Sorption fitting curves and results are shown in Figure 11b and Supporting Information Table S4. From Table S4, the correlation coefficients R^2 were all larger than 0.97, indicating that damping film theory could be used to accurately predict the CO_2 sorption rate. The sorption rate of pure M2070, PL_1_M2070, and PL AC1815 was 0.03211, 0.03235, and 0.02851 min^{-1}, respectively.

From Figure 12, there are mainly three sorption sites for PLs. The first site was the ether group on the polymer chain of the PLs. The lone pair of electrons of the oxygen atom in the ether group acted as a nucleophile to attack the carbon atom on carbon dioxide to form a carboxylic acid,[60] and detailed mechanisms are shown in Figure 13. Because there was certain free space between canopy polymer chains, carbon dioxide can be squeezed out and in with the compression and expansion between polymer chains, forming the second sorption site. In addition, due to the inner well-developed pore structure of
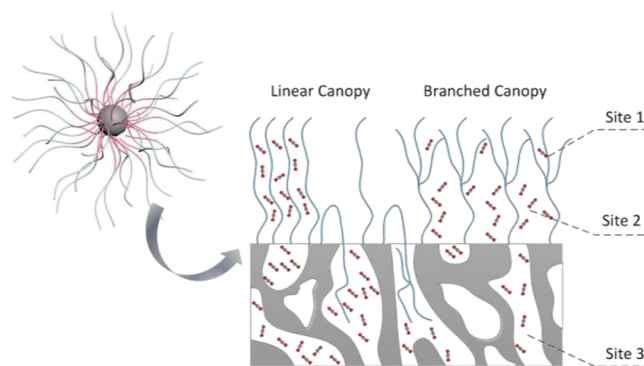
Figure 12. Schematic CO_2 sorption mechanism of porous liquids.
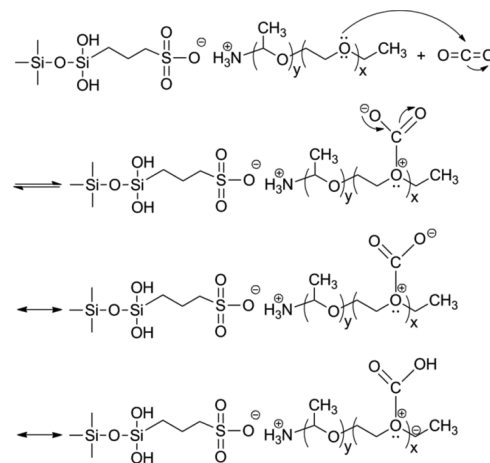
Figure 13. Schematic CO_2 sorption mechanism of the ether group in porous liquids.

PSNs, PLs could effectively adsorb carbon dioxide and form the third sorption site. Among them, the sorption of carbon dioxide on ether groups was chemisorption, and the sorption among polymer chains and the inner core was physisorption.

Figure 14 depicts the CO_2 regeneration performance of PL_1_M2070 and PL_1_AC1815. After 10 sorption/desorption cycles, PL_1_M2070 and PL_1_AC1815 retained 90.5 and 86.4% of the original CO_2 sorption capacity, respectively, demonstrating that PLs with linear canopies had better recyclability than those with branched canopies. On the one hand, the possible reason was that PLs with branched canopies were easy to enter cores, which occupied the first
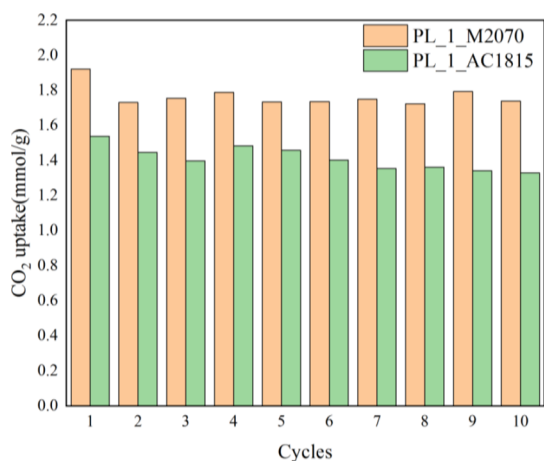
Figure 14. Recyclability of porous liquids on CO_2 sorption.

Figure 16. MSD curves of CO_2 in the porous liquid and polyetheramine at 310 K and 60 bar.

sorption site during sorption/desorption cycles. On the other hand, part carboxylic acid formed by the chemisorption could no longer reversibly form an ether group during the desorption process. Both of the two reasons resulted in the decrease in sorption capacity after 10 cycles.

4.3. Stability and Mass Transport Characteristic of the PL. In general, the unit of Type I PLs consisted of a surface-functionalized nanoparticle as a core to which selected polymers are tethered to form a canopy. Such a configuration could provide the fluidity of PLs, prevented loss of polymers, and enable PLs to exhibit near zero vapor pressure. The relative concentration curve of CO_2 and the PL in the Z axis direction is shown in Figure 15. It was clear that there was no PL molecule to vaporize to the gas reservoir because the relative concentration of PL in the gas phase was zero.

Diffusion coefficients of CO_2 in the PL and corresponding polyetheramine were obtained from the Einstein relationship at 310 K and 60 bar, which was fit by the slope of the MSD curves, as shown in Figure 16. From eq 3, the diffusion in the PL and corresponding polyetheramine was 1.23×10^{-7} and 1.27×10^{-7} m²/s, with the correlation coefficients (R^2) of 0.9987 and 0.9988, respectively. The diffusion coefficient of CO_2 in the PL was little lower than that in polyetheramine, which was mainly due to the solid content of silica cores in the PL.

5. CONCLUSIONS

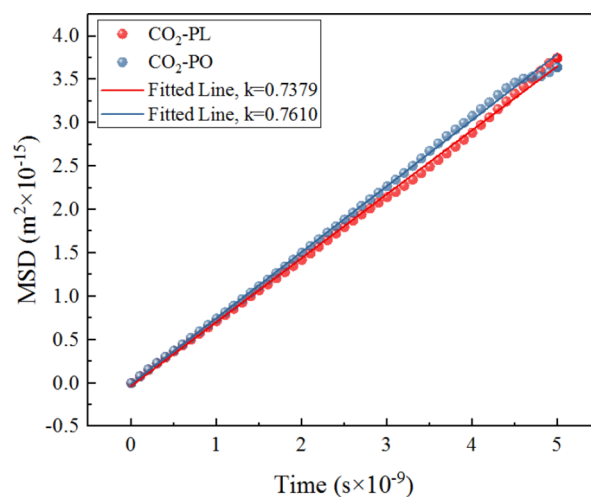In this paper, PLs with various canopy structures were successfully synthesized. A CO_2 sorption experimental station was constructed to investigate the effect of temperature, pressure, and canopy structure on CO_2 sorption capacity.

Porous materials were composed of cores, coronas, and canopies. The molecular weight of canopies should be high enough to maintain the porous materials' "liquid state" at room temperature. Characterization results of PLs revealed that the thermal decomposition temperature of PLs was nearly 100 °C higher than that of the pure canopy, which implied that the addition of cores improved thermal stability. The viscosity was affected by the branch structure and molecular weight of the canopy. Increased molecular weight was usually accompanied by entanglement, increasing flow resistance and making polymers challenging to move each other; thus, polymers with high molecular weight had higher viscosity. When branched structures existed, the possibility of entanglement between canopies was reduced, as was viscosity, and PLs had better fluidity.

CO_2 sorption capacity was affected by temperature, pressure, and canopy structures. Fitting results indicated that the pseudo-second-order kinetic model was better suited to describe the sorption behavior, which implied that the CO_2 sorption capacity of PLs was a combination of physical dissolution and chemisorption. When the temperature was raised, the solubility of CO_2 in PLs decreased, as did the saturated sorption capacity of CO_2. Furthermore, experimental results showed that the saturated sorption capacity of CO_2 increased with increasing pressure.
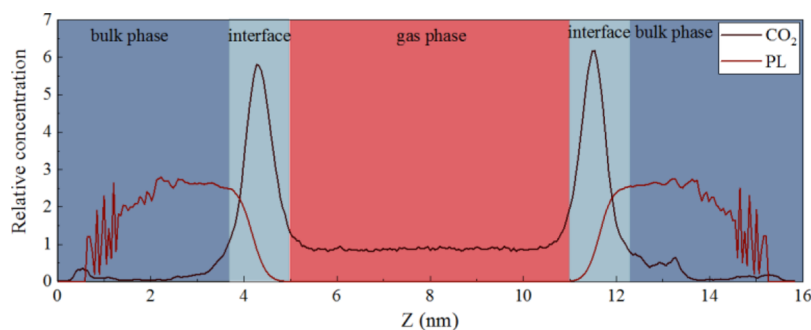

Figure 15. Relative concentration curve of CO_2 and the PL in the Z axis direction at 310 K and 60 bar.

In general, PLs with branched canopies found it easier to enter the inner cavity and occupy the CO_2 sorption site, so the amount of CO_2 absorbed by PLs with branched canopies was lower than that absorbed by PLs with linear canopies. After 10 sorption/desorption cycles, PLs retained 90.5 and 86.4% of the initial CO_2 sorption amount, indicating good recyclability.

■ ASSOCIATED CONTENT

ⓢ Supporting Information

The Supporting Information is available free of charge at https://pubs.acs.org/doi/10.1021/acsomega.1c05091.

CO$_2$ sorption/desorption experiments and calculation method, equilibrium criterion of MD simulations, part structure characterization of porous silica nanoparticles, and kinetic model parameters for CO_2 sorption in porous liquids fitted by the pseudo-first-order model and pseudo-second-order model (PDF)

■ AUTHOR INFORMATION

Corresponding Author

Zhenqian Chen − *School of Energy and Environment, Southeast University, Nanjing 210096, P. R. China; Key Laboratory of Energy Thermal Conversion and Control of Ministry of Education, Nanjing 210096, P. R. China; Jiangsu Province Key Laboratory of Solar Energy Science and Technology, Nanjing 210096, P. R. China*; Email: zqchen@seu.edu.cn

Authors

Lisha Sheng − *School of Energy and Environment, Southeast University, Nanjing 210096, P. R. China; Key Laboratory of Energy Thermal Conversion and Control of Ministry of Education, Nanjing 210096, P. R. China;* ⓞ orcid.org/0000-0002-3887-3689

Xin Wang − *School of Energy and Environment, Southeast University, Nanjing 210096, P. R. China; Key Laboratory of Energy Thermal Conversion and Control of Ministry of Education, Nanjing 210096, P. R. China*

Abdul Samad Farooq − *Institute of Refrigeration and Cryogenics, Shanghai Jiao Tong University, Shanghai 200240, P. R. China;* ⓞ orcid.org/0000-0002-4123-1062

Complete contact information is available at:
https://pubs.acs.org/10.1021/acsomega.1c05091

Author Contributions

L.S. contributed to methodology, data curation, writing and original draft preparation, visualization, and experiment. Z.C. contributed to methodology, funding acquisition, project administration, and conceptualization. X.W. helped with validation and experiment. A.S.F. helped with draft modification.

Notes

The authors declare no competing financial interest.

■ ACKNOWLEDGMENTS

■ REFERENCES

(1) Hautier, Y.; Tilman, D.; Isbell, F.; Seabloom, E. W.; Borer, E. T.; Reich, P. B. Anthropogenic environmental changes affect ecosystem stability via biodiversity. *Science* **2015**, *348*, 336−340.

(2) Muradov, N. Z.; Veziroglu, T. N. "Green" path from fossil-based to hydrogen economy: An overview of carbon-neutral technologies. *Int. J. Hydrogen Energy* **2008**, *33*, 6804−6839.

(3) Mishra, N. K.; Patil, N.; Yi, S. L. Highly selective hollow fiber membranes for carbon capture via in-situ layer-by-layer surface functionalization. *J. Membr. Sci.* **2021**, *633*, No. 113981.

(4) Ban, Y. L.; Li, Z. J.; Li, Y. S.; Peng, Y.; Jin, H.; Jiao, W. M.; Guo, A.; Wang, P.; Yang, Q. Y.; Zhong, C. L. Confinement of ionic liquids in nanocages: tailoring the molecular sieving properties of ZIF-8 for membrane-based CO_2 capture. *Angew. Chem., Int. Ed. Engl.* **2016**, *54*, 15483−15487.

(5) Tan, Y. T.; Nookuea, W.; Li, H. L.; Thorin, E.; Yan, J. Y. Property impacts on Carbon Capture and Storage (CCS) processes: A review. *Energy Convers. Manage.* **2016**, *118*, 204−222.

(6) Pera-Titus, M. Porous inorganic membranes for CO_2 capture: present and prospects. *Chem. Rev.* **2014**, *114*, 1413−1492.

(7) Kodasma, R.; Fermoso, J.; Sanna, A. Li-LSX-zeolite evaluation for post-combustion CO_2 capture. *Chem. Eng. J.* **2019**, *358*, 1351−1362.

(8) Zhang, Z. J.; Nguyen, H. T. N.; Miller, S. A.; Ploskonka, A. M.; DeCoste, J. B.; Cohen, S. M. Polymer−Metal−Organic Frameworks (polyMOFs) as water tolerant materials for selective carbon dioxide separations. *J. Am. Chem. Soc.* **2016**, *138*, 920−925.

(9) Kong, X. Y.; Li, S. S. Y.; Strmme, M.; Xu, C. Synthesis of Porous Organic Polymers with Tunable Amine Loadings for CO_2 Capture: Balanced Physisorption and Chemisorption. *Nanomaterials* **2019**, *9*, 1020.

(10) Huang, K.; Zhang, J. Y.; Liu, F. J.; Dai, S. Synthesis of porous polymeric catalysts for the conversion of carbon dioxide. *ACS Catal.* **2018**, *8*, 9079−9102.

(11) Huang, K.; Liu, F.; Dai, S. Solvothermal synthesis of hierarchically nanoporous organic polymers with tunable nitrogen functionality for highly selective capture of CO_2. *J. Mater. Chem. A* **2016**, *4*, 13063.

(12) Liu, F. J.; Huang, K.; Wu, Q.; Dai, S. Solvent-free self-assembly to the synthesis of nitrogen-doped ordered mesoporous polymers for highly selective capture and conversion of CO_2. *Adv. Mater.* **2017**, *29*, No. 1700445.

(13) Chen, C. W.; Huang, H.; Yu, Y. K.; Shi, J. W.; He, C.; Albilali, R.; Pan, H. Template-free synthesis of hierarchical porous carbon with controlled morphology for CO_2 efficient capture. *Chem. Eng. J.* **2018**, *353*, 584−594.

(14) Liu, M. Q.; Shao, L. S.; Huang, J. H.; Liu, Y. N. O-containing hyper-cross-linked polymers and porous carbons for CO_2 capture. *Microporous Mesoporous Mater.* **2018**, *264*, 104−111.

(15) Huang, K.; Liu, F. J.; Fan, J. P.; Dai, S. Open and hierarchical carbon framework with ultra-large pore volume for efficiently capture of carbon dioxide. *ACS Appl. Mater. Interfaces* **2018**, *10*, 36961−36968.

(16) Peng, H. L.; Zhang, J. B.; Zhang, J. Y.; Zhong, F. Y.; Wu, P. K.; Huang, K.; Fan, J. P.; Liu, F. J. Chitosan-derived mesoporous carbon with ultrahigh pore volume for amine impregnation and highly efficient CO_2 capture. *Chem. Eng. J.* **2019**, *359*, 1159−1165.

(17) Shen, Z. F.; Cai, Q.; Yin, C. C.; Xia, Q. N.; Cheng, J.; Li, X.; Wang, Y. G. Facile synthesis of silica nanosheets with hierarchical pore structure and their amine-functionalized composite for enhanced CO_2 capture. *Chem. Eng. Sci.* **2020**, *217*, No. 115528.

(18) Wang, Y. S.; Jia, H.; Gong, H.; Zhou, L. F.; Qiu, Z. Y.; Fang, X.; Du, T. Fabrication of trimodal porous silica/g-C3N4 nanotubes for efficient visible light photocatalytic reduction of CO_2 to ethanol. *Chem. Eng. J.* **2021**, *426*, No. 130877.

(19) Rochelle, G. T. Amine Scrubbing for CO_2 Capture. *Science* **2009**, *325*, 1652−1654.

(20) Huttenhuis, P. J. G.; Agrawal, N. J.; Solbraa, E.; Versteeg, G. F. The solubility of carbon dioxide in aqueous N -methyldiethanolamine solutions. *Fluid Phase Equilib.* **2008**, *264*, 99−112.

(21) Favre, E.; Svendsen, H. F. Membrane contactors for intensified post-combustion carbon dioxide capture by gas−liquid absorption processes. *J. Membr. Sci.* **2012**, *407*, 1−7.

(22) Zhang, W. D.; Jin, X. H.; Tu, W. W.; Ma, Q.; Mao, M. L.; Cui, C. H. Development of MEA-based CO_2 phase change absorbent. *Appl. Energy* **2017**, *195*, 316−323.

(23) Kim, I.; Svendsen, H. F. Heat of absorption of carbon dioxide (CO_2) in monoethanolamine (mea) and 2-(aminoethyl)ethanolamine (AEEA) solutions. *Ind. Eng. Chem. Res.* **2007**, *46*, 5803−5809.

(24) O'Reilly, N.; Giri, N.; James, S. L. Porous liquids. *Chemistry* **2007**, *13*, 3020−3025.

(25) Sheng, L. S.; Chen, Z. Q.; Xu, B.; Shi, J. Molecular dynamics simulations of stability and fluidity of porous liquids with different canopy structures. *J Phys. Chem. B* **2021**, *46*, 5387−5396.

(26) Sheng, L. S.; Chen, Z. Q.; Wang, Y. Molecular dynamics simulations of stability and fluidity of porous liquids. *Appl. Surf. Sci.* **2021**, *536*, No. 147951.

(27) Sheng, L. S.; Chen, Z. Q. Molecular dynamics study of dispersion and fluidity of porous liquids with different pore sizes. *J. Mol. Liq.* **2021**, *333*, No. 115890.

(28) James, S. L. The dam bursts for porous liquids. *Adv. Mater.* **2016**, *28*, 5712−5716.

(29) Atwood, J. L.; Barbour, L. J.; Jerga, A.; Schottel, B. L. Guest transport in a nonporous organic solid via dynamic van der Waals cooperativity. *Science* **2002**, *298*, 1000−1002.

(30) Hemming, E. B.; Masters, A. F.; Maschmeyer, T. The encapsulation of metal nanoparticles within porous liquids. *Chem. Commun.* **2019**, *55*, 11179−11182.

(31) Zhang, J. S.; Chai, S. H.; Qiao, Z. A.; Mahurin, S. M.; Chen, J. H.; Fang, Y. X.; Wan, S.; Nelson, K.; Zhang, P. F.; Dai, S. Porous Liquids: A promising class of media for gas separation. *Angew. Chem., Int. Ed.* **2014**, *54*, 932−936.

(32) Li, P. P.; Schott, J. A.; Zhang, J. S.; Mahurin, S. M.; Sheng, Y. J.; Qiao, Z. A.; Hu, X. X.; Cui, G. K.; Yao, D. D.; Brown, S.; et al. Electrostatic-assisted liquefaction of porous carbons. *Angew. Chem., Int. Ed.* **2017**, *56*, 14958−14962.

(33) Deng, Z.; Ying, W.; Gong, K.; Zeng, Y. J.; Yan, Y. G.; Peng, X. H. Facilitate gas transport through metal-organic polyhedra Constructed Porous Liquid Membrane. *Small* **2020**, *16*, No. 1907016.

(34) Atilhan, M.; Cincotti, A.; Aparicio, S. Nanoscopic characterization of type II porous liquid and its use for CO_2 absorption from molecular simulation. *J. Mol. Liq.* **2021**, *330*, No. 115660.

(35) Egleston, B. D.; Luzyanin, K. V.; Brand, M. C.; Clowes, R.; Briggs, M. E.; Greenaway, R. L.; Cooper, A. I. Controlling gas selectivity in molecular porous liquids by tuning the cage window size. *Angew. Chem., Int. Ed.* **2020**, *59*, 7362−7366.

(36) Greenaway, R. L.; Holden, D.; Eden, E. G. B.; Stephenson, A.; Yong, C. W.; Bennison, M. J.; Hasell, T.; Briggs, M. E.; James, S. L.; Cooper, A. I. Understanding gas capacity, guest selectivity, and diffusion in porous liquids. *Chem. Sci.* **2017**, *8*, 2640−2651.

(37) Zhang, F.; Yang, F. C.; Huang, J. S.; Sumpter, B. G.; Qiao, R. Thermodynamics and kinetics of gas storage in porous liquids. *J. Phys. Chem. B* **2016**, *120*, 7195−7200.

(38) Melaugh, G.; Giri, N.; Davidson, C. E.; James, S. L.; Del Popolo, M. G. Designing and understanding permanent microporosity in liquids. *Phys. Chem. Chem. Phys.* **2014**, *16*, 9422−9431.

(39) Shan, W. D.; Fulyio, P. F.; Kong, L. Y.; Schott, J. A.; Do-Thanh, C. L.; Tian, T.; Hu, X. X.; Mahurin, S. M.; Xing, H. B.; Dai, S. New class of Type III porous liquids: a promising platform for rational adjustment of gas sorption behavior. *ACS Appl. Mater. Interfaces* **2017**, *10*, 32−36.

(40) Liu, S. J.; Liu, J. D.; Hou, X. D.; Xu, T. T.; Tong, J.; Zhang, J. X.; Ye, B. J.; Liu, B. Porous liquid: a stable ZIF-8 colloid in ionic liquid with permanent porosity. *Langmuir* **2018**, *34*, 3654−3660.

(41) Knebel, A.; Bavykina, A.; Datta, S. J.; Sundermann, L.; Garzon-Tovar, L.; Lebedev, Y.; Durini, S.; Ahmad, R.; Kozlov, S. M.; Shterk, G.; et al. Solution processable metal−organic frameworks for mixed matrix membranes using porous liquids. *Nat. Mater.* **2020**, *19*, 1346−1353.

(42) Cahir, J.; Tsang, M. Y.; Lai, B. B.; Hughes, D.; Alam, M. A.; Jacquemin, J.; Rooney, D.; James, S. L. Type 3 porous liquids based

on non-ionic liquid phases-a broad and tailorable platform of selective, fluid gas sorbents. *Chem. Sci.* **2020**, *11*, 2077−2084.

(43) Zhao, X. M.; Yuan, Y. H.; Li, P. P.; Song, Z. J.; Ma, C. X.; Pan, D.; Wu, S. D.; Ding, T.; Guo, Z. H.; Wang, N. A polyether amine modified metal organic framework enhanced the CO_2 sorption capacity of room temperature porous liquids. *Chem. Commun.* **2019**, *55*, 13179−13182.

(44) Giri, N.; Davidson, C. E.; Melaugh, G.; Del Popolo, M. G.; Jones, J. T. A.; Hasell, T.; Cooper, A. I.; Horton, P. N.; Hursthouse, M. B.; James, S. L. Alkylated organic cages: from porous crystals to neat liquids. *Chem. Sci.* **2012**, *3*, 2153−2157.

(45) Giri, N.; Del Popolo, M. G.; Melaugh, G.; Greenaway, R. L.; Ratzke, K.; Koschine, T.; Pison, L.; Gomes, M. F. C.; Cooper, A. I.; James, S. L. Liquids with permanent porosity. *Nature* **2015**, *527*, 216−220.

(46) Mastalerz, M. Materials chemistry: Liquefied molecular holes. *Nature* **2015**, *527*, 174−175.

(47) Li, H.; Gao, X. T.; Jia, C. Z.; Chen, W.; Liu, B.; Yang, L. Y.; Sun, C. Y.; Chen, G. J. Enrichment of Hydrogen from a Hydrogen/ Propylene Gas Mixture Using ZIF-8/Water-Glycol Slurry. *Energies* **2018**, *11*, 1890.

(48) Li, X. Q.; Ding, Y. D.; Guo, L. H.; Liao, Q.; Zhu, X.; Wang, H. Non-aqueous energy-efficient absorbents for CO_2 capture based on porous silica nanospheres impregnated with amine. *Energy* **2019**, *171*, 109−119.

(49) Jie, K. C.; Onishi, N.; Schott, J. A.; Popovs, I.; Jiang, D. E.; Mahurin, S.; Dai, S. Transforming Porous Organic Cages into Porous Ionic Liquids via a Supramolecular Complexation Strategy. *Angew. Chem., Int. Ed.* **2020**, *59*, 2268−2272.

(50) Wang, T. Y.; Jiang, H. T.; Zhao, Q. F.; Wang, S. L.; Zou, M. J.; Cheng, G. Enhanced mucosal and systemic immune responses obtained by porous silica nanoparticles used as an oral vaccine adjuvant: Effect of silica architecture on immunological properties. *Int. J. Pharm.* **2012**, *436*, 351−358.

(51) Plazinski, W.; Rudzinski, W.; Plazinska, A. Theoretical models of sorption kinetics including a surface reaction mechanism: A review. *Adv. Colloid Interface Sci.* **2009**, *152*, 2−13.

(52) Ding, Y. D.; Guo, L. H.; Li, X. Q.; Liao, Q.; Zhu, X.; Wang, H. CO_2 absorption of anhydrous colloidal suspension based silica nanospheres with different microstructures. *Energy Environ.* **2020**, *32*, 1437−1456.

(53) Liu, Y. M.; Yu, X. J. Carbon dioxide sorption properties and sorption/desorption kinetics of amine-functionalized KIT-6. *Appl. Energy* **2018**, *211*, 1080−1088.

(54) Ho, Y. S.; Mckay, G. Sorption of dye from aqueous solution by peat. *Chem. Eng. J.* **1998**, *70*, 115−124.

(55) Shi, T.; Zheng, Y. P.; Wang, T. Y.; Li, P. P.; Wang, Y. D.; Yao, D. D. Effect of pore size on the carbon dioxide sorption behavior of porous liquids based on hollow silica. *ChemPhysChem* **2018**, *19*, 130−137.

(56) Wang, D. C.; Xin, Y. Y.; Li, X. Q.; Wang, F.; Wang, Y. D.; Zhang, W. R.; Zheng, Y. P.; Yao, D. D.; Yang, Z. Y.; Lei, X. F. A universal approach to turn UiO-66 into Type 1 porous liquids via post-synthetic modification with corona-canopy species for CO_2 capture. *Chem. Eng. J.* **2020**, *416*, No. 127625.

(57) Park, Y.; Petit, C.; Han, P.; Park, A. H. A. Effect of canopy structures and their steric interactions on CO_2 sorption behavior of liquid-like nanoparticle organic hybrid materials. *RSC Adv.* **2014**, *4*, 8723−8726.

(58) Bourlinos, A. B.; Simopoulos, A.; Petridis, D. Synthesis of capped ultrafine γ-fe2o3 particles from iron(iii) hydroxide caprylate: a novel starting material for readily attainable organosols. *Chem. Mater.* **2002**, *14*, 899−903.

(59) Zhang, F.; Gao, K. X.; Meng, Y. N.; Qi, M.; Geng, J.; Wu, Y. T.; Zhang, Z. B. Intensification of dimethyaminoethoxyethanol on CO2 absorption in ionic liquid of amino acid. *Int. J. Greenhouse Gas Control* **2016**, *51*, 415−422.

(60) Sharma, P.; Choi, S. H.; Park, S. D.; Baek, I. H.; Lee, G. S. Selective chemical separation of carbondioxide by ether functionalized

imidazolium cation based ionic liquids. *Chem. Eng. J.* **2012**, *181*, 834–841.